

Turbulent outflows from [WC]-type nuclei of planetary nebulae^{*}

I. BD +30°3639 and other [WC 9–10] stars

Y. Grosdidier^{1,2,3,**}, A. Acker¹, and A.F.J. Moffat^{2,3,***}

¹ Observatoire Astronomique de Strasbourg, UMR 7550, 11 rue de l'Université, 67000 Strasbourg, France (yvesgro@astro.u-strasbg.fr; acker@astro.u-strasbg.fr)

² Université de Montréal, Département de Physique, C.P. 6128, Succursale Centre-Ville, Montréal (Québec) H3C 3J7, Canada (moffat@astro.umontreal.ca; yves@astro.umontreal.ca)

³ Observatoire du mont Mégantic, Canada

Received 4 February 2000 / Accepted 28 September 2000

Abstract. Using spectroscopic observations taken at the Observatoire de Haute-Provence (OHP, France) and the European Southern Observatory (ESO, Chile), we describe wind fluctuations in four [WC 9–10]-type central stars of planetary nebulae, especially BD +30°3639, which was observed intensively during 15 nights. Moving features seen on the top of the C III λ 5696 emission line are interpreted as outflowing “blobs” which are radially accelerated outwards, as seen in the winds of massive Wolf-Rayet stars. We find line profile variations occurring on a time scale of hours. Kinematic parameters of the blobs are derived and compared to those of massive Wolf-Rayet stars. The wind fragmentation process appears independent of the strong differences between both types of hot stars.

Key words: ISM: planetary nebulae: individual: BD +30°3639 – ISM: planetary nebulae: individual: He 2-99 – ISM: planetary nebulae: individual: He 2-142 – ISM: planetary nebulae: individual: Sw St 1 – stars: mass-loss – turbulence

1. Introduction

1.1. Hot stars showing the Wolf-Rayet phenomenon

Among the ~ 1500 known Galactic planetary nebulae (PN), ~ 350 show a detectable stellar continuum. From the latter subset, ~ 50 nuclei show broad emission line-spectra of the Wolf-Rayet (WR) carbon sequence (Acker et al. 1992; Tylenda et al. 1993; Peña et al. 1998). The majority of these central stars are distributed among the [WC 2–4] and [WC 8–11] spectral

types, with only a few stars belonging to intermediate classes (Acker et al. 1996, 2000a). Recall that no WN central star of a planetary nebula has been detected so far. It is worthy of note that Population I & II WC stars of the same subtype are virtually indistinguishable on the basis of their stellar spectra alone (Méndez et al. 1991). Additional criteria are required to discriminate between Population I & II WC stars: e.g. absolute luminosities or linear radii of the surrounding nebulae (both are significantly smaller for Population II — i.e. low-mass — WC stars).

For both Population I & II WC stars, line formation is normally assumed to arise in a (roughly) spherically expanding atmosphere, where non-LTE conditions (Leuenhagen & Hamann 1994; Leuenhagen et al. 1996) and possibly similar wind radiative/hydrodynamic instabilities prevail (e.g. Owocki et al. 1988; Owocki 1994; Feldmeier 1995). The cool subclasses of Population II [WC] stars are close to the entry point into the WR phase, subsequent evolution likely occurring to earlier, hotter subtypes via the mass-loss peeling-off process *and/or* convective mixing and subsequent burning: post-Asymptotic Giant Branch (AGB) \rightarrow [WC]-late \rightarrow [WC]-early \rightarrow PG 1159 (Feibelman 1999; Koesterke & Hamann 1997; Acker et al. 1996). On the other hand, massive, Population I WR stars of the carbon sequence are believed to follow a similar evolutionary scenario, WC-late \rightarrow WC-early (Moffat 1995).

1.2. Fragmented, radiatively driven winds

Moving subpeaks are systematically seen on the tops of broad optical emission lines from massive WR stars (Robert 1992; Lépine & Moffat 1999, and references therein). These subpeaks suggest WR winds/atmospheres are *inhomogeneous* and *non-stationary* (on a time-scale of hours). This is supported by at least four additional facts (e.g. see Moffat 1996): i) the observed red line wings due to electron scattering are significantly weaker than the wings modeled under the hypothesis of a smooth wind (Hillier 1984; Hillier 1991); ii) the observed slopes of the radio and infrared continua are not reproduced in

Send offprint requests to: Yves Grosdidier

^{*} Mainly based on observations taken at the Observatoire de Haute-Provence, France, and on some observations obtained at the European Southern Observatory, Chile (ESO Prog. IDs: 57.C-0492, 59.C-0293, 61.C-0512).

^{**} Present address: Instituto de Astrofísica de Canarias, Calle Vía Láctea s/n, 38200 La Laguna (Tenerife), Spain

^{***} Killam Fellow of the Canada Council for the Arts.

Correspondence to: Yves Grosdidier

the homogeneous atmosphere model for WR winds (Lamers & Waters 1984; Runacres & Blomme 1996; Blomme & Runacres 1997); iii) polarimetric and photometric, stochastic variabilities (Brown et al. 1995; Robert et al. 1989) are observed on a time-scale similar to that of the optical emission lines; and iv) when more than two ionizing stages of the same element are observed, atmosphere models assuming homogeneity fail to reproduce *simultaneously* all these lines: an increased (decreased) density region favours the population of lower (higher) ionizing stages. Given the $\sim r^{-2}$ density stratification and outward decreasing temperature distribution of the global wind, we expect the emission lines of both lower and higher ionization stages to reach more comparable intensities when *local* density enhancements are additionally involved (however, quantitative assessments of the latter phenomenon often require a precise knowledge of the line formation mechanisms).

Furthermore, evidence is mounting that *all* fast, hot winds are *potentially* inhomogeneous. Indeed, recently, a search for similar spectroscopic variations was conducted for [WC] nuclei of PN, both by Balick et al. (1996) and Grosdidier et al. (1997), showing evidence for a clumpy wind in the vicinity of NGC 40's [WC 8] central star. Later, first results of an observational search for wind variability in [WC 9] central stars led to a detection of wind fluctuations in the spectrum of BD +30°3639 (Acker et al. 1997). Similarly, time series of very high signal-to-noise ratio, high-resolution spectra of the He II λ 4686 emission line in the O4I(n)f supergiant ζ Puppis have been obtained by Eversberg et al. (1998). In the latter study, the authors detected stochastic, variable substructures in the line, like those observed in the winds of massive WR stars, which are probably the descendants of O and Of stars. Therefore, evidence is accumulating that wind clumping may be an *intrinsic* characteristic of all radiatively driven stellar winds.

In this series of papers, we investigate the manifestation of wind clumping originating in some PN nuclei showing the Wolf-Rayet phenomenon. We perform comparisons with the wind clumping exhibited by their massive WR counterparts, leading to a more general, universal description of the wind fragmentation process as a purely atmospheric wind phenomenon: despite the strong differences between both types of hot stars, we show that the spectroscopic variability is quite similar.

In this first paper (Paper I), we report line-profile variations in optical emission lines of BD +30°3639 and three other — less intensively observed — [WC 9–10]-type central stars of PN. In the second paper of this series (Grosdidier et al. 2000, hereafter Paper II) we will concentrate on a particular [WC]-late type central star, the [WC 8] nucleus of the planetary nebula NGC 40. Subsequent papers will discuss the case of early [WC]-type nuclei.

2. Observations and data reduction

The four program stars are listed in Table 1, which gives in Column (1) the PN and central star designations; in Column (2) the spectral type and V magnitude of the central star; in Column (3) the telescope and spectrograph used; in Column (4)

the observed spectral range, the adopted spectral resolution and resolving power (RP); in Column (5) the continuum signal-to-noise ratios for each night given in Column (6); in Column (6) the dates of observation; in Column (7) the integration time of each spectrum; in Column (8) the number of spectra acquired each night.

In order to resolve the narrow subpeaks present on the tops of the emission lines, it is necessary to have a spectral resolution of ~ 0.5 – 1 Å, or better. On the other hand, the subpeaks are very weak, and securing time resolution along with sufficient S/N ratio imposes the use of very large telescopes. As a compromise in this study, we concentrate on the relatively bright [WC 9] central star of He 2-438, BD +30°3639, observed intensively (15 nights) with a 2 m class telescope. The less frequent observations obtained for the three other [WC 9–10]-type central stars are preliminary. We concentrate on the C III λ 5696 emission line because it is very bright for [WC 9] stars and free from any blending. It is the best line to study expanding stellar wind variability.

For BD +30°3639 we used the 1.52 m telescope at the Observatoire de Haute-Provence (OHP, France) equipped with the Aurélie spectrograph (see Gillet et al. 1994). The detector was a double linear array Thomson TH7832 of 2048 pixels (see Gillet et al. 1994, and references therein). We used a 600 l/mm grating, leading to a 2.8-pixel resolving power of 11000 (~ 0.5 Å spectral resolution at 5500 Å). The spectral range is centered on 5750 Å and covers 5500–5950 Å. The entrance aperture of Aurélie is circular with a diameter of 3''.

For the southern objects we used the 1.4 m Cassegrain Auxiliary Telescope (CAT) at the European Southern Observatory (ESO, Chile) combined with the Coudé Echelle Spectrometer (CES). The detector was CCD LO#38 (Loral) with 2688×512 pixels. The CES has a classical Czerny-Turner grating mount with an échelle grating of 79 l/mm as the dispersive element, leading to a 4.8-pixel resolving power of 50000 (~ 0.1 Å spectral resolution at 5700 Å). The spectral range, centered on 5695 Å, covers 5670–5720 Å. The width of the slit was 2.5''.

We carried out a first preliminary study on BD +30°3639 in 1996 March 1–6 (3 spectra of 20–30 minutes each) at the OHP, where we detected significant spectral variability of the C III λ 5696 and C IV λ 5801/12 emission lines. Then we observed this star more intensively in May 1996. The results from the May run are presented in Acker et al. (1997). On the other hand, preliminary observations were performed by François Cuisinier in 1996 July 15 (6 consecutive spectra of 40 minutes exposure each) on the central star of He 2-99, with the 1.52 m ESO telescope equipped with the B&C spectrograph at low resolution ($RP = 1500$). These spectra show significant variability of the C III λ 5696 emission line. All these observations encouraged us to study these two central stars (He 2-99 at higher resolution) and others, in order to resolve the subpeaks overlying the C III λ 5696 emission line.

The spectra were reduced in the usual way with the MIDAS¹ package: bias subtraction, flat field correction, and wave-

¹ <http://www.eso.org/projects/esomidias/>

length calibration using an Argon-Thorium lamp. Flux calibrations were performed for the BD +30°3639 runs using the standard stars HR 3454 and HR 5511. Finally, the spectra were normalized to the continuum. Imperfect guiding or centering and variable seeing (typically 2–3") remove stellar light but not nebular light from the slit. Therefore, rectification of the stellar continuum to unity permitted us to get reliable and comparable stellar emission line measurements. Such a procedure allows one to study subtle changes in emission lines, as was shown by Robert (1992), Lépine & Moffat (1999), Eversberg et al. (1998), and references therein. No attempt was made to subtract nebular contributions due to lines or continuum, because they do not disturb the C III λ 5696 stellar line profile.

3. The [WC 9] central star of He 2-438: BD +30°3639

3.1. Introduction

The central star of this PN is the brightest known northern [WC] star, and appears in a large number of publications (611 references were found, in the years 1893 to 2000, from SIMBAD²).

He 2-438 is a low excitation nebula that recently emerged from the Asymptotic Giant Branch (AGB) stage: IR spectroscopic modelling during the post-AGB evolution by Siebenmorgen et al. (1994) led to an age of only ~ 900 years after the end of the AGB mass-loss stage, a value in fairly good agreement with the kinematic expansion age of about 500 years (see Acker et al. 1998).

Hubble Space Telescope images reveal small-scale (~ 0.2 arcsec) clumps and filaments in [O II] λ 3727 and [S III] λ 9532 (see Arnaud et al. 1996; Harrington et al. 1997). As pointed out by these authors, a part of the clumpy structure is caused by a non-uniform distribution of dust in the neutral halo (inferred from comparison of the [O II] and [S III] images corresponding to, respectively, high and low extinction zones). The radio (VLA+MERLIN) 6 cm-images confirm a clumpy structure (Bryce et al. 1997). Near- and mid-IR images allow one to determine the source of IR excess: it appears that one component of the excess is located near the central star and is possibly due to non-equilibrium heating of small grains.

ASCA X-ray data show the presence of a bubble of hot (3×10^6 K) plasma dominated by He-burning products, although O is not as abundant as in the star's wind itself (see Arnaud et al. 1996). These authors noted that the properties of the hot wind-blown bubble are in conflict with the predictions of a simple interacting wind-model: i) thermal pressure in the wind-blown bubble is almost an order of magnitude higher than the pressure within the ionized shell — these pressures should be nearly equal in the interacting-wind model; ii) the temperature is about 10 times lower than expected for a zone post-shocked by the 600–700 km s⁻¹ stellar wind. Arnaud et al. (1996) propose that the low temperature might result either from mixing of the shocked stellar wind with the material photo-evaporated from clumps left behind the expanding shell within the hot bubble, or more likely from rapid variations in the stellar wind properties.

Such rapid changes are also compatible with the fact that the stellar mass-loss rate ($\sim 1.3 \times 10^{-5} M_{\odot} \text{ yr}^{-1}$; Leuenhagen et al. 1996), combined with the terminal velocity $v_{\infty} \approx 600\text{--}700$ km s⁻¹, could fill the bubble in only $\sim 10^1$ years, which is a very short time-scale.

Recent studies confirm the assumption of variations in the stellar wind properties: HIPPARCOS photometric monitoring shows that the luminosity of BD +30°3639 increased over 3 years by about 0.1 mag (see Fig. 1 in Acker et al. 1998). This variation is compatible with the different values of V given in the literature (from 9.5 to 12.5; see Acker et al. 1998 and references therein). The central star of He 2-438, BD +30°3639, was included in Balick et al.'s study (1996), but no spectroscopic flickering was detected at their chosen resolution ($\sim 1.5 \text{ \AA}$).

3.2. Results

Several kinds of features are visible in the observed spectra: i) Broad emission features formed in the stellar wind. The lines of He, C and O are broadened due to the motion of the expanding stellar wind. Some of the emissions are accompanied by blue-shifted absorption troughs (P-Cygni profiles); ii) Narrow emission lines which are formed in the planetary nebula; iii) Interstellar absorption features. See Fig. 1.

3.2.1. Line profile variations

In Fig. 2, differences from the mean profile (calculated from the whole set of spectra obtained in 15 nights; see lower panels) of the C III λ 5696 emission line are shown as a function of time for two typical observing nights at the OHP (upper panels). The segment in the lower right corner of the upper panel indicates the amplitude for 0.25 (apparent) continuum units in the residuals. This amplitude does not take into account the change of intensity across the emission line and relative to the adjacent continuum. True amplitudes relative to the continuum will be estimated in Sect. 3.2.2.

In order to emphasize the trajectories of subpeaks on the top of the C III λ 5696 line, Fig. 3 shows grayscale plots of nightly differences from the global mean profile for the 14 nights, made up of at least 4 individual spectra. The global mean profile is presented in the lower panels, and gaps within the time series appear as a black horizontal bar. These plots were obtained via an interpolation both in the wavelength and the time domains of the nightly data. The interpolation along the time domain compensates for the small gaps/delays between individual spectra.

The characteristic time scale for significant variations is confirmed to be a few hours. Ejection times and starting wavelengths of individual blobs appear at random (this is shown more clearly in Fig. 5 in a subsequent section) which suggests a turbulent origin. The strongest, most obvious features appear to last longer and move throughout the C III line with *apparently* constant acceleration. The range of measured accelerations will be presented in Sect. 3.2.3. For six nights within the whole 15 night set (1996 May 15, 20 & 21; 1996 August 9; 1997 July 26 & 30), a simple glance at the grayscale plots shows only slight accel-

² <http://simbad.u-strasbg.fr/Simbad>

Table 1. Sample of observed Wolf-Rayet central stars of planetary nebulae and log of spectroscopic observations.

| Denomination | Central star | | Journal of observations | | | | |
|--------------------|--------------|-------------------|-------------------------|-----------------|-------------|-------------|---------|
| | | | Spectr. range | S/N^b | Date | Expos. time | N° of |
| Usual name PN | Spectr. type | Telescope (diam.) | Spectr. resol. (RP) | | | (min.) | spectra |
| Star name(s) | V^a | Spectrograph | | | | | |
| (1) | (2) | (3) | (4) | (5) | (6) | (7) | (8) |
| 064.7+05.0 | [WC 9] | OHP (1.52 m) | 5500–5950 Å | 19–25 | 1996 May 15 | 25 | 6 |
| He 2-438 | 9.92 | AURELIE | ~0.5 Å (11000) | 20–24 | 1996 May 17 | 25 | 8 |
| BD +30°3639 | | | | 23–29 | 1996 May 20 | 25 | 9 |
| HD 184738 | | | | 20–24 | 1996 May 21 | 25 | 4 |
| V 1966 Cyg | | | | 22–29 | 1996 Aug 7 | 30 | 3 |
| | | | | 27–39 | 1996 Aug 8 | 30 | 8 |
| | | | | 32–46 | 1996 Aug 9 | 30 | 8 |
| | | | | 29–42 | 1996 Aug 11 | 30 | 11 |
| | | | | 27–43 | 1996 Aug 12 | 30 | 11 |
| | | | | 30–40 | 1996 Aug 13 | 30 | 11 |
| | | | | 32–41 | 1997 Jul 26 | 30 | 13 |
| | | | | 35–47 | 1997 Jul 27 | 30 | 13 |
| | | | | 25–45 | 1997 Jul 28 | 30 | 12 |
| | | | | 40–50 | 1997 Jul 29 | 30 | 12 |
| | | | | 16–32 | 1997 Jul 30 | 30 | 8 |
| 309.0-04.2 | [WC 9] | ESO/CAT (1.4 m) | 5670–5720 Å | NA ^c | 1997 Jun 27 | 90 | 1 |
| He 2-99 | 14.0 | CES-long camera | ~0.1 Å (50000) | NA | 1997 Jun 28 | 120 | 3 |
| LSS 3169 | | | | NA | 1997 Jun 29 | 120 | 3 |
| | | | | NA | 1997 Jun 30 | 120 | 3 |
| | | | | NA | 1997 Jul 1 | 120 | 3 |
| | | | | NA | 1997 Jul 2 | 120 | 3 |
| 001.5-06.7 | [WC 9–10] | ESO/CAT (1.4 m) | 5670–5720 Å | 30–35 | 1997 Jun 27 | 60 | 2 |
| Sw St 1 | 11.8 | CES-long camera | ~0.1 Å (50000) | | | | |
| HD 167362 | | | | | | | |
| 327.1-02.2 | [WC 9] | ESO/CAT (1.4 m) | 5670–5720 Å | NA ^c | 1997 Jun 27 | 90 | 2 |
| He 2-142 | 15.1 | CES-long camera | ~0.1 Å (50000) | | | | |

^a From the Acker et al. (1992) catalogue, but for BD +30°3639 the V value is from Acker et al. (1998).

^b Characteristic signal-to-noise ratio evaluated in the continuum adjacent to C III λ 5696.

^c Irrelevant, the continuum is underexposed.

erations compared to the behaviour of the subpeaks during the other nights. We will discuss this finding in a following section.

If the blobs are observed in lines with quite different formation *loci*, one may be able to estimate their true characteristic lifetimes. In this way, it should also be possible to convincingly test the hypothesis of supersonic, compressible turbulence. Unfortunately, the insufficient S/N in the higher ionization C IV λ 5801/12 emission feature prevents us from clearly identifying moving features (in any case, its blending complicates such identifications). For the other (weak) lines, the situation is even worse; most of the apparent subpeaks arising from noise can be erroneously associated with true manifestations of local overdensities. The need for échelle observations over long time intervals and at *very high* S/N with large telescopes is required to address the question of the origin of the clumps.

The terminal velocity (in the outer line formation region) was estimated from the broadening of the C III λ 5696 emission line. The terminal velocity (expressed in km s^{-1}) is correlated with the $FWHM$ (expressed in Å) of the C III line via (Torres et al. 1986):

$$v_{\infty} = \left(\frac{FWHM}{5696} \right) \times c \times 0.9,$$

where c is the velocity of light.

This holds quite well for massive WC 9 stars, for which the C III λ 5696 emission is nearly Gaussian. Assuming this relation also holds for [WC 9] stars, it yields: $v_{\infty} = 580\text{--}600 \text{ km s}^{-1}$, for $FWHM \approx 12.2\text{--}12.7 \text{ Å}$ (the range being determined from the whole set of our spectra).

3.2.2. Level of variability

A simple inspection by eye of Fig. 2 or Fig. 3 is sufficient to roughly deduce the temporal behavior of the line profile variations. However, the precise characterization of these variations could be greatly influenced by photon statistics and other sources of error in the region of interest. In order to rigorously estimate the significance level of the line profile variations (lpv), we applied the “temporal variance spectrum” analysis (TVS) of Fullerton et al. (1996).

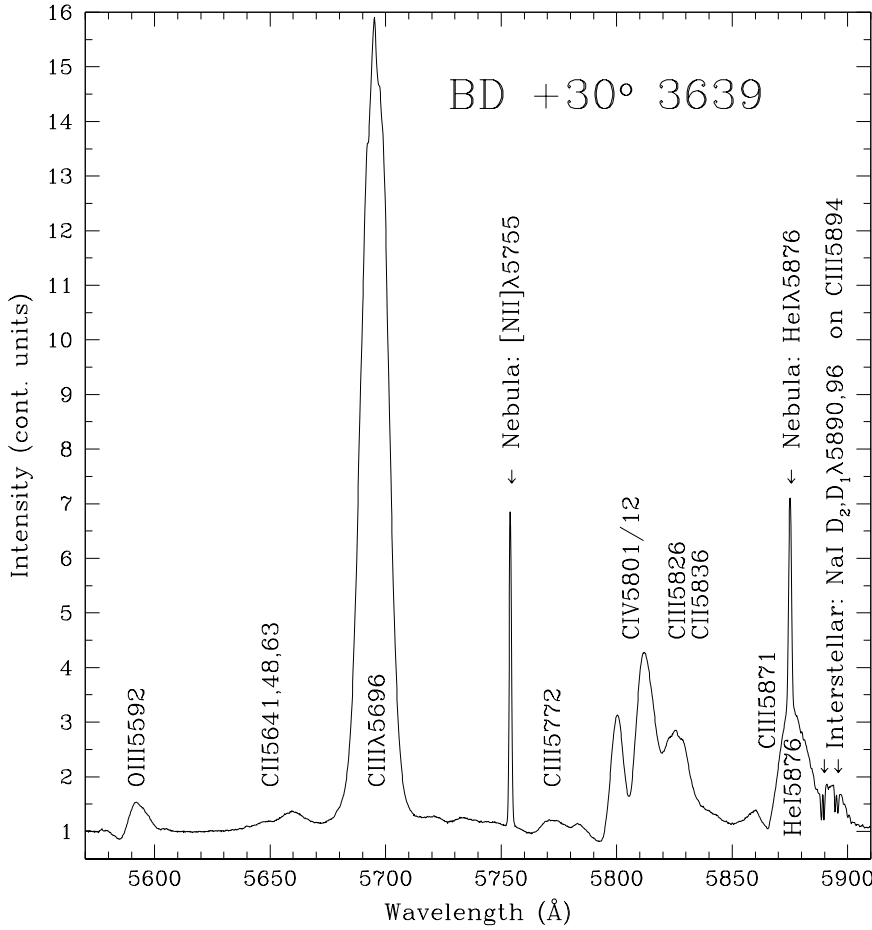


Fig. 1. A typical normalized spectrum of BD +30° 3639 indicating the most obvious emission or absorption features (1997 July 27).

In order to describe the lpv for a collection of N spectra of a given star, we placed the N rectified spectra in a matrix S_{ij} , where i and j denote the spectrum (=time) and the pixel (=wavelength bin) indices, respectively. After that, we produced a reference spectrum \bar{S}_j as a mean weighted by the signal-to-noise in the continuum associated with each individual exposure. Then we calculated the weighted differences:

$$d_{ij} = \frac{\sigma_{0j}}{\sigma_{ij}} \times (\bar{S}_j - S_{ij}),$$

where σ_{0j} is the reciprocal of the rms S/N of the spectral time series (see Fullerton et al. 1996), and σ_{ij} are the elements of the matrix giving the noise associated with the element S_{ij} . In our case (relatively large signal-to-noise ratios and moderate readout noise), we can reasonably assume that σ_{ij} is given by Poisson statistics, i.e., by the square root of the count number (in electrons) accumulated at a given pixel/wavelength bin. Then, we can assume that the individual d_{ij} are drawn from the same nearly Gaussian population: $N(0, \sigma_{0j})$. The overall variation for a collection of N spectra follows:

$$TVS_j = \frac{1}{N-1} \sum_{i=1}^N \left[\frac{d_{ij}}{\sigma_{0j}} \right]^2.$$

Thus the TVS retains its simple $\chi^2_{N-1}/(N-1)$ distribution for all pixels j because the individual d_{ij}/σ_{0j} are drawn from a

reduced centered normal Gaussian distribution (Fullerton et al. 1996).

Roughly speaking, the values of the TVS give a statistical assessment of the variability level at a given wavelength. Indeed, the deviations of the time variations across the lines are computed with proper weights to account for the changes in the signal-to-noise ratios across the lines and from one spectrum to the next. Since the statistical behaviour of the temporal variability under the null hypothesis of no variability is described by the $\chi^2_{N-1}/(N-1)$ distribution, contours of equal probability can be plotted along with each TVS. Here, these contours are simply \sim horizontal lines since our spectral range is quite small with a nearly constant S/N ratio across each spectrum ($\sigma_{0j} \approx \text{const.}, \forall j$). Whenever the TVS exceeds a contour, this signifies a sufficiently unlikely value (the small tail of probability p), i.e. the null hypothesis can be rejected in favour of its alternative: significant variability. Accounting for the noise level in the line profile, any value of TVS above this threshold ensures that the line-profile variability is significant at the $p\%$ level.

In the following, the values of the deviations from a template-weighted mean spectrum are expressed in percentage of the normalized continuum flux through: $\sigma_{0j} \times (TVS_j)^{1/2}$.

In order to assess the significance of the lpv, we then compare the values of $\sigma_{0j} \times (TVS_j)^{1/2}$ with:

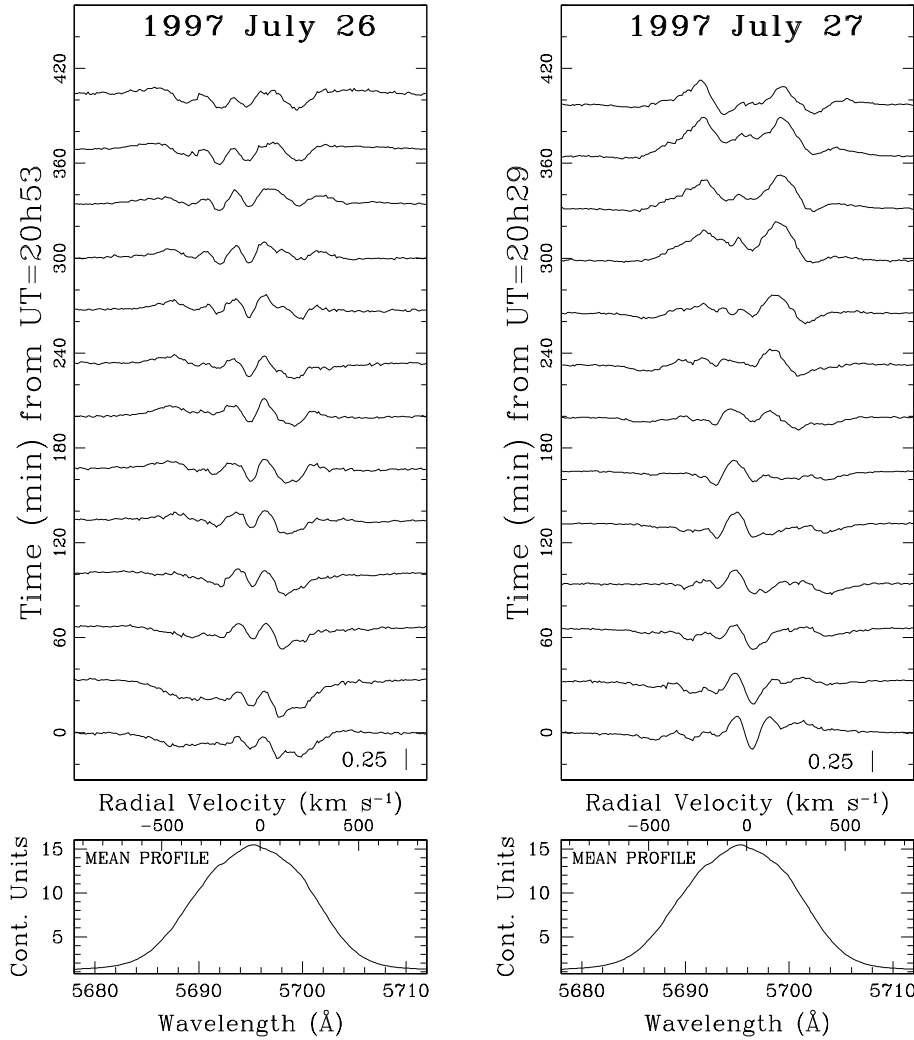


Fig. 2. Residuals from the mean of C III λ 5696 in BD +30°3639 for 1997 July, 26 and 27. The segment in the lower right corner of the upper panel indicates the amplitude for 0.25 (apparent) continuum units in the residuals. Velocities are given in the stellar rest frame. The mean profile in the bottom panels is based on all the spectra in 15 nights.

$$\sigma_{0j} \times \left[\frac{\chi_{N-1}^2}{N-1} \right]^{\frac{1}{2}}$$

The temporal variance spectra have been calculated for each of the 7 nights made up of at least 11 individual spectra, in order to secure statistical significance. Fig. 4 shows the related TVS along with contour levels for significant variability at 1% & 5% levels. For the TVS of the 1996 May run, the reader is referred to Acker, Grosdidier & Durand (1997). To facilitate the identification of the variable zones, the nightly mean spectra are superposed. The main results are the following:

1. All obvious emission lines within our spectral range are variable at the 1% level.
2. In the case of the O III λ 5592 emission line, the variations are mainly detected only in its blue-shifted absorption component (up to 5–6% of the continuum flux on 1997 July 26 & 28, and 1996 August 12). However, its emission component exhibits remarkably similar variations on 1997 July 26. This suggests huge variations in the *whole* line formation region, rather than only along the line of sight.
3. The emission component of He I λ 5876 generally exhibits variability from 4–5%, up to \sim 11% of the continuum flux

on 1997 July 26. However, the absorption component is always variable (5–7% of the continuum flux), although this variability is only marginally detected on 1996 August 11.

4. The complex C IV λ 5801/12 is always variable with amplitudes reaching 5–7% of the continuum flux, and up to 10–12% during the 1997 July run. The 1997 July 26 night appears to be associated with an intense, persistent burst of activity lasting the subsequent nights, judging by the magnitude of the TVS in that spectral region.
5. The C III λ 5696 line shows huge variability of 15–20% of the continuum flux, the maximum being detected on 1997 July 26 (\sim 25%) and correlated with a burst of C IV λ 5801/12 (\sim 12%). In addition, the entire line shows prominent variability, suggesting blobs/inhomogeneities propagating into the whole line emission region.
6. The 1997 July period of intense activity compared to the 1996 August run does not show significant changes in the global line strengths, except for He I λ 5876 emission, which appears somewhat intensified in 1997. This could be associated with a decrease of the wind temperature, or with an increase of wind density. We favor the decrease of the local wind temperature because any increase of the wind density

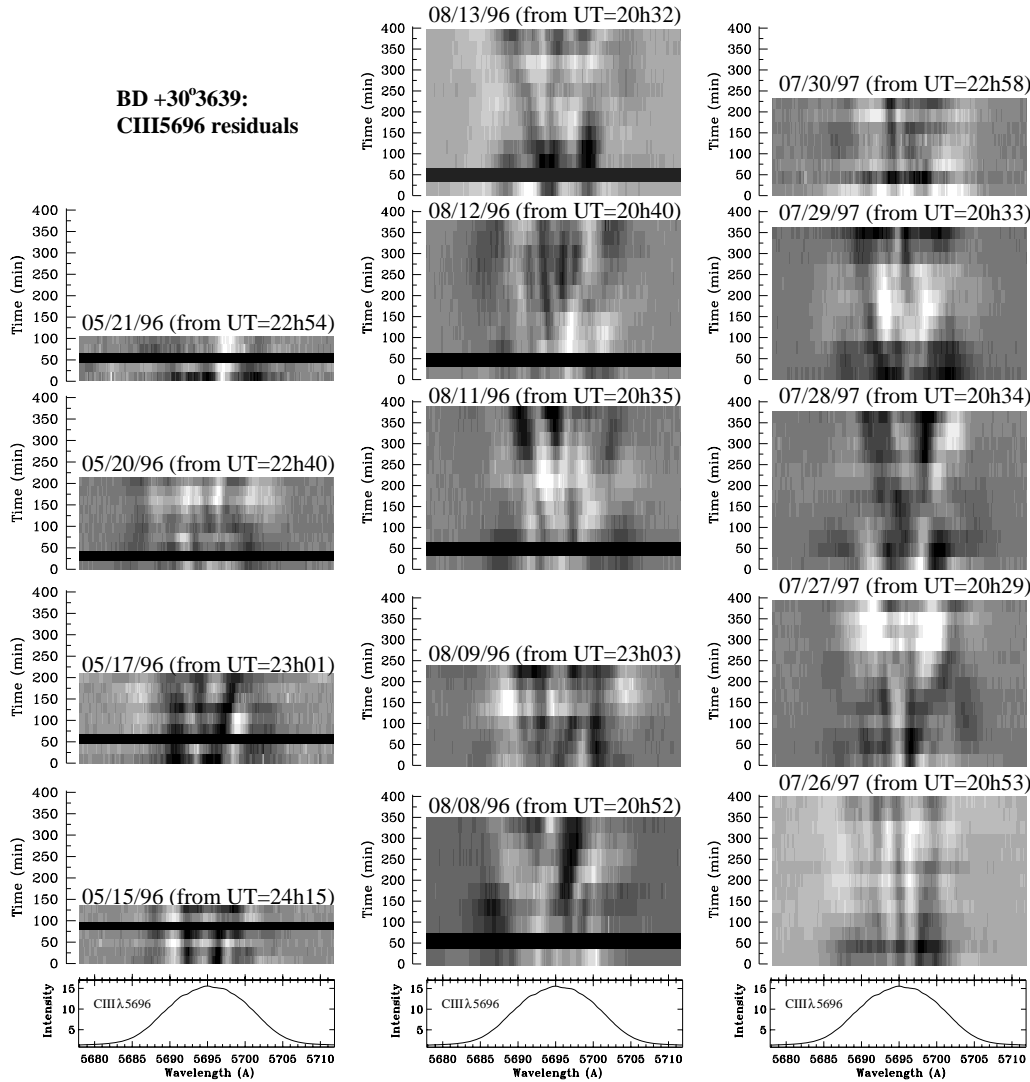


Fig. 3. Grayscale plots for BD +30°3639 of C III λ 5696 residuals for 14 nights. Bottom panels show the 15-night mean. The range of the grayscale plots is -1.0 (black, lack of emission) to 1.0 (white, excess of emission) continuum units.

results in an increase in the line optical depths, which results in a decrease of the radiative acceleration in the supersonic region. A decrease in the radiative acceleration implies a lower terminal velocity, which is not detected (the *FWHM* of the emission lines appear to be nearly constant).

- As was already noticed for massive WR stars, the blue-shifted absorption component of the lines exhibiting P-Cygni profiles in BD +30°3639 is significantly more variable than the emission component. This is likely mainly due to the small volume of matter in front of the stellar “disk”, making it more sensitive to relative fluctuations. This suggests linear sizes for the blobs of $\sim 1 R_*$ as was already suggested by Lépine & Moffat (1999) from their phenomenological simulations of variable emission profiles: they have estimated the number of local overdensities in the line formation region to be of the order of 10^{3-4} . Taking into account the size of the line emission region, we infer linear sizes of the overdensities to be $\lesssim 1 R_*$.

Note that the huge variability of the nebular lines (O I λ 5577, [N II] λ 5755 and He I λ 5876) are illusory. They are caused by

imperfect guiding and variable seeing, both of which remove stellar light but not nebular light from the slit, in combination with rectification of the stellar continuum to unity. The nebular line raw data show no significant variability.

One may notice the extremely good wavelength calibration from inspection of the nebular and interstellar lines. The Na I D doublet (rest wavelengths at 5890 and 5896 Å) is clearly visible in all OHP/BD +30°3639 spectra, where two different components can be identified. Nebular as well as interstellar lines are perfectly superposed on the nightly mean spectra. This is supported by the tightness of their related temporal variance spectra.

3.2.3. Kinematics of the subpeaks

The subpeaks generally show measurable velocity shifts during their lifetime, although during some nights they appear to rest roughly at the same wavelengths. For the intense features (representing an apparent excess of emission as well as an apparent deficit of emission in the difference spectra) seen on at least three consecutive spectra, we measured mean radial velocities v_R and

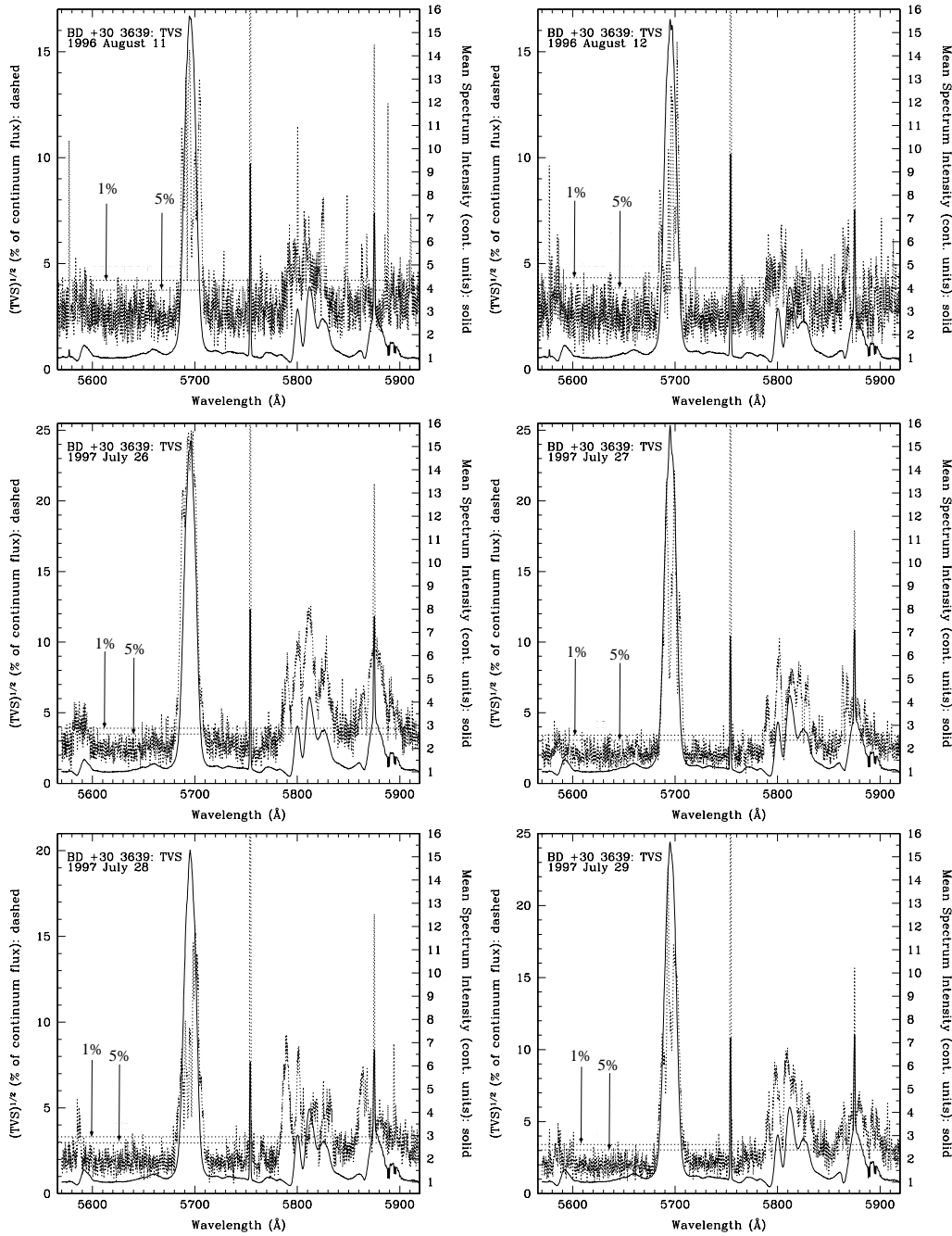


Fig. 4. BD +30°3639 nightly mean spectra (solid lines) and the computed square root of the TVSs (dashed lines), for 6 nights (see text). Contours of statistical significance for 1% and 5% levels are indicated by horizontal dotted lines (see arrows). Our calculations account for pixel-to-pixel and spectrum-to-spectrum differences in the noise distribution. For 1996 August 13, the behaviour of BD +30°3639 is essentially similar to that of the two other nights of the August run.

computed the related mean radial accelerations $a_R = dv_R/dt$ through linear fits. Fig. 5 summarizes the results for 85 extracted features, on which theoretical (a_R, v_R) -relations (derived from the beta velocity-law) are plotted (see Sect. 3.2.4). Horizontal error bars reflect the observed *range* of radial velocities for a single blob, whereas vertical error bars show the dispersion ($\pm 1\sigma$) of possible accelerations derived from the linear fits. The spread in v_R values suggests that the starting and ending wavelengths appear at random.

Because $a_R \times v_R \geq 0$ for the large majority of the blobs, Fig. 5 suggests that the assumption of *outwardly* radially accelerating features is quite reasonable. However, 4 structures (only

one at more than 2σ) move towards line centre. These structures may be related to nonradial pulsations, local wind rotation motions, or orbital motions, since all these processes could involve subpeak motions towards the line centre. However, their small number (less than 5% of the total set of 85 structures) suggests that they are probably spurious, being the tail end of a statistical distribution. Starting and ending wavelengths of individual blobs seem to appear at random, and suggests a chaotic variability taking on different time-scales.

The a_R values seem to be slightly concentrated towards low radial accelerations. This fact, combined with the short time coverage of series/nights 1996 May 15, 20 & 21, and 1996 August

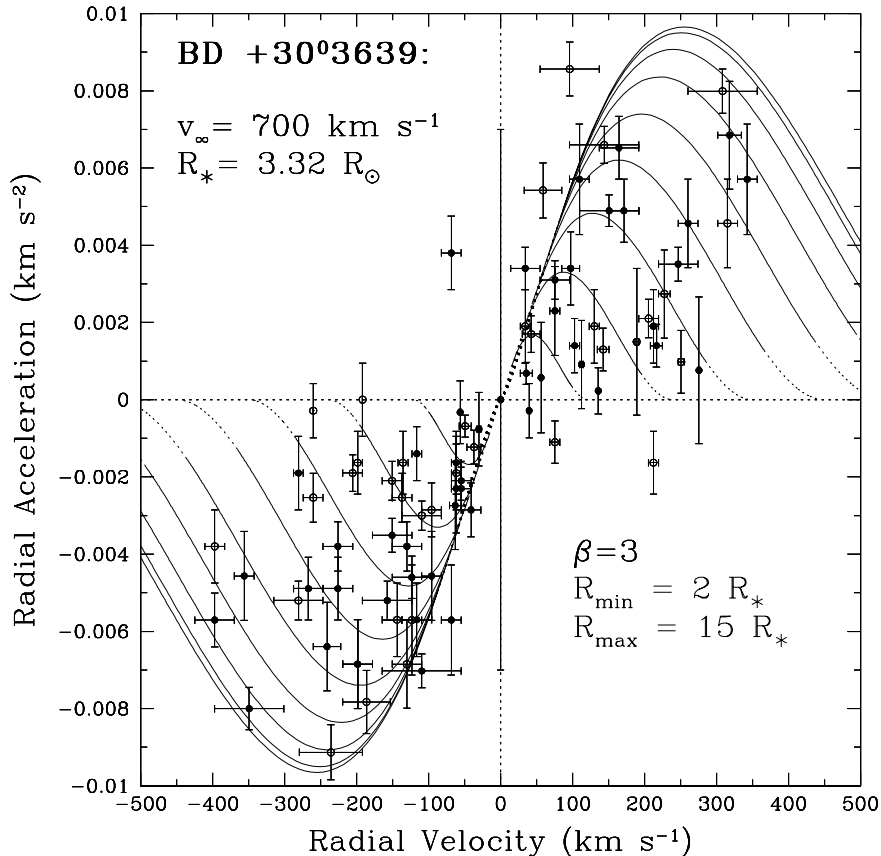


Fig. 5. Kinematics in the form of projected mean acceleration vs projected mean velocity for each subpeak/gap on top of the C III λ 5696 emission line (85 points). Filled (open) symbols correspond to an excess (deficit) of emission. The projected β -velocity law is shown for $\theta = 0^\circ$ (towards the observer, lower left corner) to 180° (away from the observer, upper right corner), in steps of 10° ($R_{min} \leq r \leq R_{max}$: solid curves; $r < R_{min}$ and $r > R_{max}$: dotted lines). We use the stellar parameters given by Leuvenhagen et al. (1996); see text.

9, would explain why we only detect small accelerations during these four nights. On the other hand, the 1997 July 26 (~ 400 min monitoring) and 1997 July 30 (~ 250 min monitoring) series are quite long. For the latter nights, the absence of large accelerations seems to be real and significant. There are at least three explanations for the low accelerations detected during these two nights: i) a temporary decrease in the direct stellar radiation³ (Owocki & Puls 1999, and references therein); ii) a temporary increase in the diffuse radiation within the stellar wind (Owocki & Puls 1999, and references therein); or, more likely, a statistical effect. The latter effect is as follows: Lépine & Moffat (1999) showed that the number of local elementary overdensities in the line formation region would be at least 10^{3-4} . However, many overdensities spanning large radial distances (hence different spatial velocities $v(r)$) may show the same v_R . The number of local overdensities responsible for one single subpeak may be at least 10^{2-3} (Lépine 1999; private communication). Therefore, at a given wavelength and at a given time, one may measure a mean radial acceleration which is fixed by the current spatial distribution of the overdensities within the line formation region (hence probing different acceleration regimes). If the velocity law of the wind is monotonic, one may detect only slight mean accelerations around $|v_R| \approx 0$ and towards line wings, and larger accelerations in between. Therefore, the low accel-

erations measured during the 1997 July 26 and 1997 July 30 nights point to a transient anisotropic distribution of the overdensities within the line formation region.

Acceleration moduli range from nearly 0 to 9 m s^{-2} . The global mean radial acceleration is $3.6 \pm 0.8 \text{ m s}^{-2}$. Overall, these values are very similar to those observed in the massive WC 9 star WR 103 (see Robert 1992; Lépine & Moffat 1999). Thus the wind fragmentation process appears to be a purely atmospheric wind phenomenon, despite the strong differences between both types of hot stars.

3.2.4. Kinematics of the subpeaks: Comparison with the β -velocity field

For comparison, the theoretical (a_R, v_R) -relation derived from the β velocity field, $v(r) = v_\infty(1 - R_*/r)^\beta$, is also plotted in Fig. 5 for different angles θ between the line of sight and blob directions of movement ($v_R = v(r) \cos(\theta)$, $a_R = dv_R/dt$). The maximum acceleration occurring in a β velocity field is given by:

$$a_{max} = k(\beta) \frac{v_\infty^2}{R_*}, \quad (1)$$

with

$$k(\beta) = 4\beta \frac{(2\beta - 1)^{2\beta - 1}}{(2\beta + 1)^{2\beta + 1}}, \quad (2)$$

³ Unfortunately, because the OHP sky is not photometric, our absolute flux calibrations are not reliable to test for subtle changes in the continuum emission.

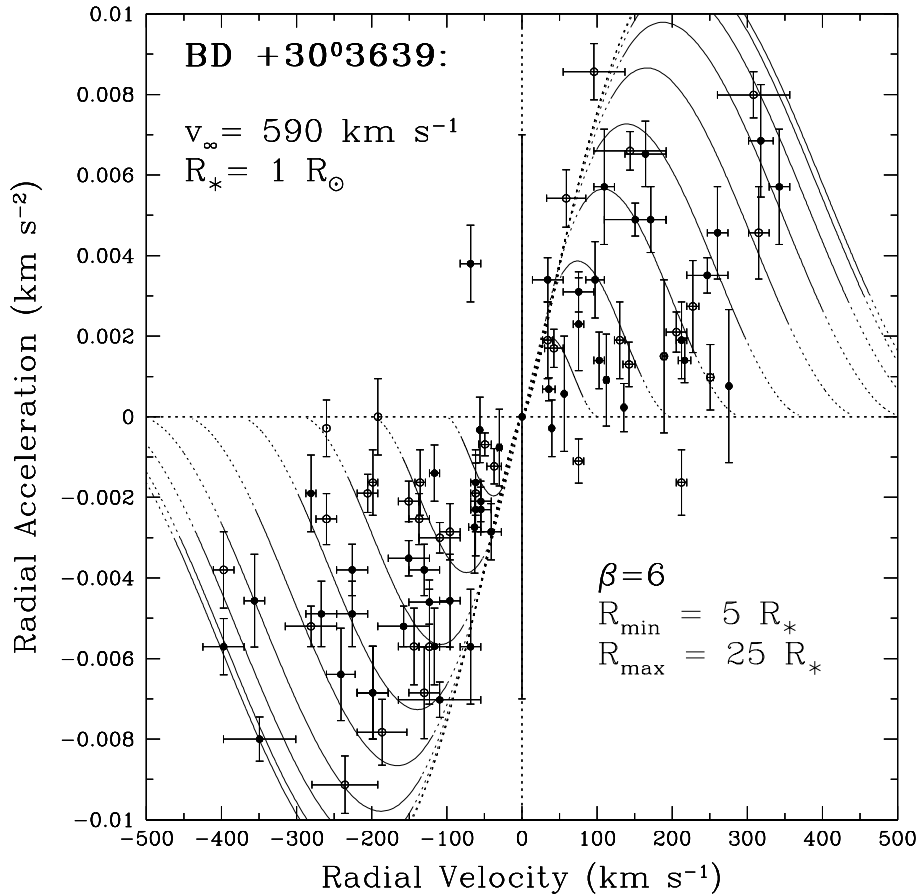


Fig. 6. Same as Fig. 5: here, we use our v_∞ value determined in Sect. 3.2.1 and guess a stellar radius of $1 R_\odot$ for BD +30°3639; see text.

the function k being nearly independent of β for β above 2–3. In addition, this maximum acceleration $da/dr = 0$ occurs at the radial distance $r = r_{max} = (\beta + 1/2)R_*$.

Adopting $v_\infty = 700 \text{ km s}^{-1}$ and $R_* = 3.32 R_\odot$ for BD +30°3639 (Leuhenagen et al. 1996), the kinematics are consistent with a β velocity law with $\beta \approx 3$, in contrast to the value $\beta = 1$ adopted in the atmosphere model (Leuhenagen et al. 1996). Indeed, a β value as small as 1 is ruled out because it would imply accelerations ranging up to $\sim 31 \text{ m s}^{-2}$ (Eqs. (1) and (2)) which are not observed!

With $\beta = 3$, the line formation region is evaluated to span radial distances 2–15 R_* from the nucleus, judging from the distribution of the data in Fig. 5. Since the lifetime of the subpeaks is a few hours, they cross, at speed $\sim 600 \text{ km s}^{-1}$, a zone limited to about a few tenths of the line formation region in radial extension. Thus the wind of BD +30°3639 is highly variable on a *very short time-scale*, which supports a turbulent origin.

Within the accuracy of our measurements and despite the generally *poor* reliability of stellar radii estimates from atmosphere models, $R_* \approx 3 R_\odot$ is an appropriate value for the stellar radius *with* $\beta = 3$: smaller stellar radii (as expected for progenitors of white dwarfs) would imply larger accelerations, which are also not observed. Indeed, for $\beta \approx 2$ –3, the maximum acceleration occurs at about 2 stellar radii above the star’s surface and $k(\beta) \approx 0.04$ –0.07. A stellar radius as small as $0.5 R_\odot$ is ruled out because it would imply accelerations (for $\beta = 2$ –3)

ranging up to 50–100 m s^{-2} , which are about 7–15 times higher than the observed *maximum* values.

Recall Lépine & Moffat (1999) who noticed that for $\beta > 1$ a measure of the wind acceleration as a function of the velocity, combined with the knowledge of v_∞ , yields only a constraint on the product $\beta \times R_*$. Therefore, judging from the distribution of the data in Fig. 5, we estimate βR_* for BD +30°3639 to be in the range 6–15 R_\odot . For nine massive WR stars, Lépine & Moffat (1999) found $\beta R_* \approx 20$. Our lower βR_* is likely mainly related to the small radius of BD +30°3639, as expected for PN nuclei.

The true maximum acceleration is necessarily greater or equal to $(a_{max})_{obs}$, thus Eq. (1) gives us an upper boundary for R_* . Therefore, taking $\beta R_* \approx 10$, we argue that realistic β velocity fits of the actual velocity field should yield $R_* \approx 10/\beta \approx 3 R_\odot$, with $\beta \approx 3$. In other words, $R_* \approx 3 R_\odot$ being clearly too large for BD +30°3639, which is believed to be less massive than $1 M_\odot$ (Acker et al. 1998), lower stellar radii are more likely, requiring $\beta > 3$. For example, taking our estimate of the terminal velocity, $v_\infty = 590 \text{ km s}^{-1}$, and estimating $R_* = 1 R_\odot$, we can fit the observed kinematics with $\beta = 6$ (Fig. 6), in contrast with the value $\beta = 1$ adopted in the atmosphere model. As a consequence, the line formation region is now located farther out in the wind.

Our estimate of the maximum acceleration occurring within the line formation region would in principle give an additional

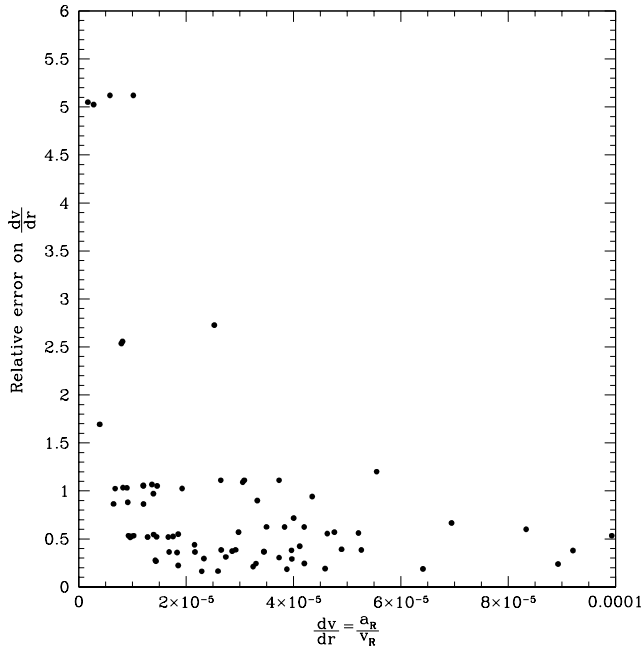


Fig. 7. Relative error on dv/dr , $\sigma(dv/dr)/(dv/dr)$, as a function of dv/dr for the blobs in Fig. 5 satisfying $a_R \times v_R \geq 0$. The horizontal axis is in s^{-1} .

constraint on R_* and β . Indeed, for the given observed $(\beta R_*)_{obs}$ and $(a_{max})_{obs}$ values, solving Eq. (1) for R_* and multiplying both the lefthand and righthand terms by β leads to:

$$(\beta R_*)_{obs} = \beta k(\beta) \frac{v_\infty^2}{(a_{max})_{obs}}. \quad (3)$$

Therefore, the combined knowledge of $(\beta R_*)_{obs}$, v_∞ and $(a_{max})_{obs}$ should give us the value of $\beta k(\beta)$, hence β . Unfortunately, the function $\beta k(\beta)$ is strongly independent of β for β above $\sim 2-3$, preventing any reliable estimation of β .

However, one should keep in mind that the above arguments rely on the correctness of the β velocity field and the possibility of extrapolating wind characteristics down to the stellar surface: i) it is well known that the β velocity law is not as realistic as desired (Springmann 1994; Gayley et al. 1995); ii) extrapolation might be very hazardous since it intrinsically assumes that wind properties and dynamics are only determined by the underlying star. We know that such an assumption does not prevail because of the ionization structure of the winds, which appear thermally stratified, with important consequences for the dynamics (e.g. Hillier 1991).

3.2.5. The velocity gradient in the line formation region

If blobs can be assumed to be good tracers of the overall wind velocity field, they give observational constraints for the accelerations occurring in different parts of the wind and then probe the *actual* velocity law within a large volume of the stellar atmosphere. Our kinematic measurements, although limited to the radial component, can even yield information on the true/observed velocity field within the line formation region.

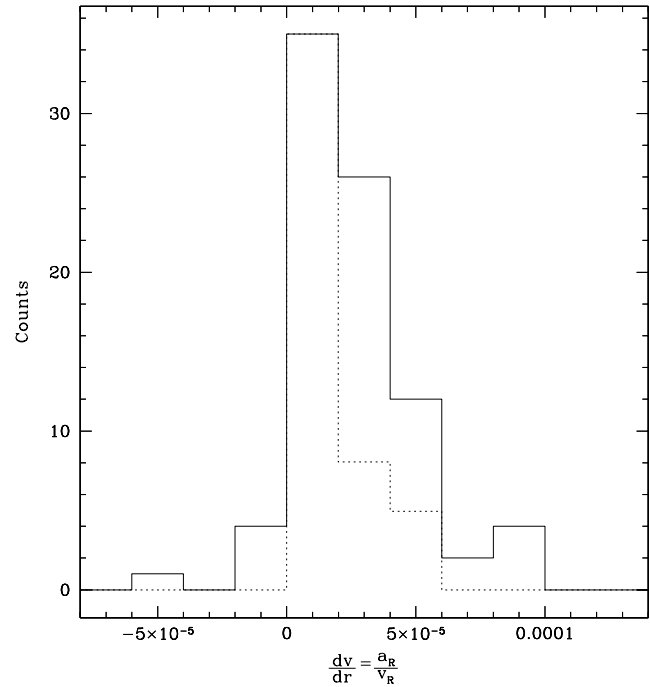


Fig. 8. Frequency distribution of the dv/dr values (solid histogram). For comparison, the distribution expected from a true β -velocity field is also plotted (dotted histogram). The line formation region in the second histogram is assumed to span radial distances 2–15 R_* from the central star (see text). The horizontal axis is in s^{-1} .

Since the observed ratio a_R/v_R reduces to dv/dr , we then considered the whole set of blobs satisfying $a_R \times v_R \geq 0$, and calculated the corresponding dv/dr . Note that the relative error on dv/dr is often quite large: see Fig. 7. However, the relatively high number of subpeaks encouraged us to perform a statistical analysis of the dv/dr derived from our kinematic measurements. Fig. 8 shows the frequency distribution of the dv/dr values (solid histogram). Large bins have been chosen in order to compensate for the large errors often encountered in evaluating the dv/dr . For comparison, the distribution expected from a purely β velocity field is also shown (dotted histogram), for the radial distances between R_{min} and R_{max} found before, $\beta = 3$, $R_* = 3.32 R_\odot$, and $v_\infty = 700 \text{ km s}^{-1}$. The latter histogram has been normalized to the values of the observed histogram at their maximum, occurring in the same bin. Note the excess of features occurring at $dv/dr > 2 \times 10^{-5} \text{ s}^{-1}$, compared to the number expected from a pure β -velocity field. Since the majority of the features showing $dv/dr > 2 \times 10^{-5} \text{ s}^{-1}$ have relative errors around 0.5, this result appears to be reliable. This suggests that the β velocity field underestimates the true gradient within the flow.

4. Other program stars

4.1. The [WC 9] nucleus of He 2-99

This planetary nebula was catalogued by Henize in 1964. Kaler et al. (1989) published a fundamental atlas of identifications for the UV and optical spectra of the $V \approx 14.0$ central star.

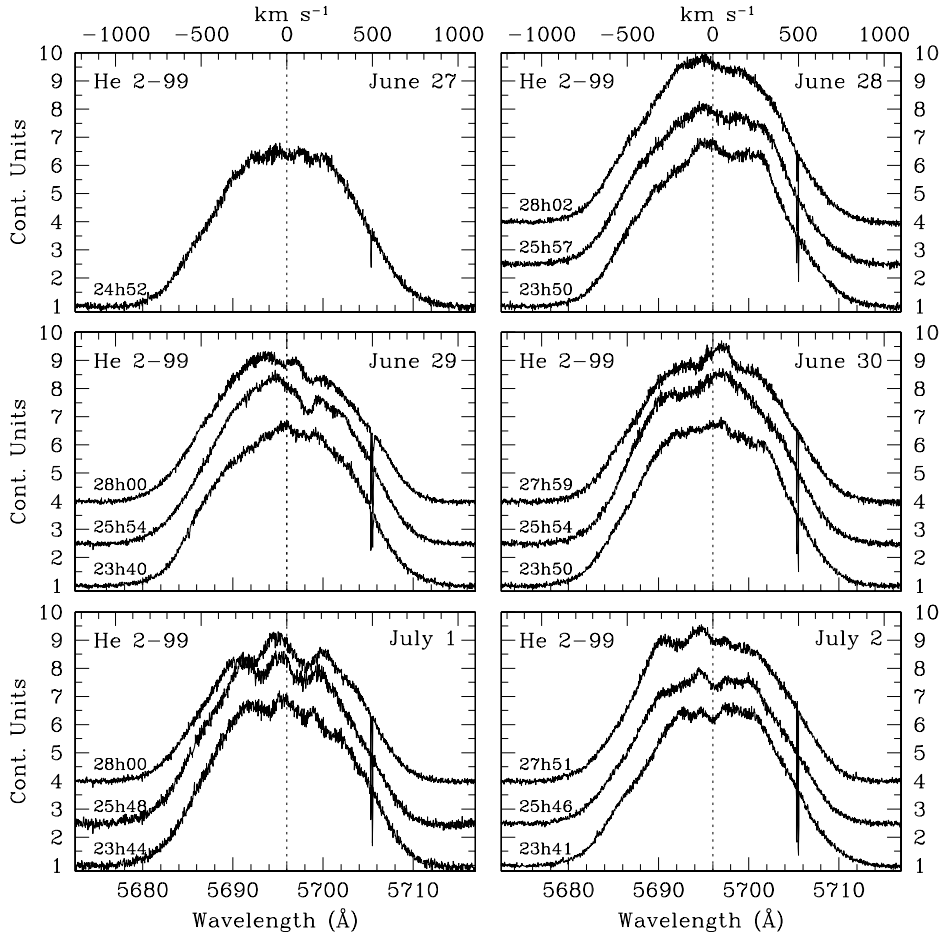


Fig. 9. Time-series of the C III λ 5696 emission line in He 2-99 for 1997 June, 27–30, and 1997 July 1–2. Velocities are given in the stellar rest frame.

Leuhenagen et al. (1996) estimate the terminal velocity to be 900 km s^{-1} from the blueshift of observed P-Cygni profiles within their atmosphere model.

Leuhenagen et al. (1996), Méndez et al. (1991) and Kaler et al. (1989) emphasized the similarity between the spectra of BD +30°3639 and the central star of He 2-99. Only two differences prevail in slightly broader emission lines and higher degree of ionization (hence higher effective temperature) in the case of He 2-99. The nebula exhibits an elliptical shape, multiple shells, numerous faint, fine structures and jet-like outflows like those of He 2-142.

Fig. 9 shows an exploratory time-series of the monitored C III λ 5696 emission line in He 2-99. This time-series is shown as a function of time for each observing night at ESO. A narrow absorption line ($\sim 5706 \text{ \AA}$) is visible on the C III λ 5696 line of He 2-99. Although this feature does not correspond to a known interstellar absorption line/band (Foing & Ehrenfreund 2000, private communication), the absence of this feature on the spectra of Sw St 1 and He 2-142 (see Figs. 11 and 12) rules out a detector defect and suggests a possible interstellar origin. As stellar continuum was underexposed, we were not able to give any reliable estimate of the line intensity. However, because the C III line is as bright as in BD +30°3639, the relatively faint central star of He 2-99 also exhibits well-exposed substructures on top of the emission line. We detect at least 8 persistent features.

The temporal variance spectrum (TVS) was calculated for the whole set of 16 spectra. Fig. 10 shows the TVS along with contour levels for significant variability at the 1% & 5% levels. The level of variability reaches 15–20% of the adjacent continuum flux, which is comparable to the level of variability exhibited by BD +30°3639.

For the detected persistent features, we report a maximum projected acceleration of about 5.6 m s^{-2} . This is comparable with the value found above for BD +30°3639.

4.2. The [WC 9] nucleus of He 2-142

This poorly known nucleus was catalogued by Henize in 1964. The nebular expansion velocity is unknown but Sahai & Trauger (1998) assumed a value of 15 km s^{-1} . This object exhibits an elliptical morphology along with numerous jet-like outflows (Sahai & Trauger 1998).

Fig. 11 presents two consecutive spectra showing the C III λ 5696 emission line in He 2-142 for 1997 June, 27. Note that the stellar continuum is underexposed and thus prevents any reliable estimate of the line intensity. However, we can detect some changes on top of the line profile, with possibly two persistent features at $\sim +200 \text{ km s}^{-1}$ and $\sim -100 \text{ km s}^{-1}$. The terminal velocity (in the outer line formation region) was estimated from the broadening of the C III λ 5696 emission line

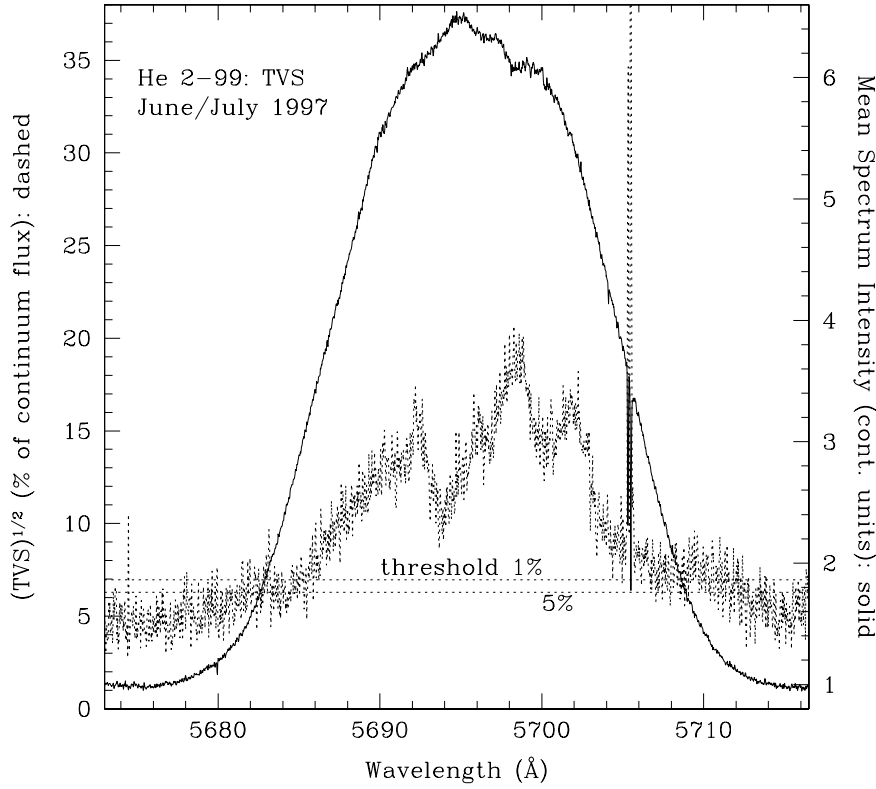


Fig. 10. He 2-99 mean spectrum (solid line) and the computed square root of the TVS (dashed line), both calculated with 16 individual spectra for 1997 June–July run. Contours of statistical significance for 1% and 5% levels are indicated by *horizontal* dotted lines. Our calculations account for pixel-to-pixel and spectrum-to-spectrum differences in the noise distribution.

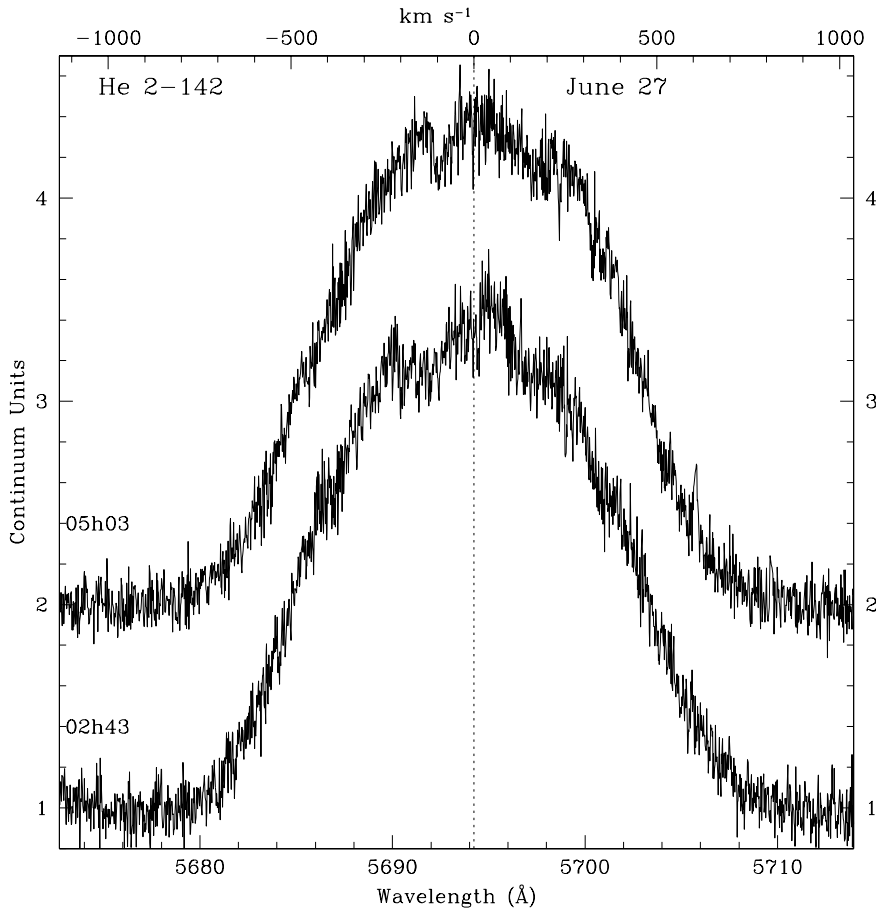


Fig. 11. Two consecutive spectra showing the C III λ 5696 emission line in He 2-142 for 1997 June, 27. Velocities are given in the stellar rest frame.

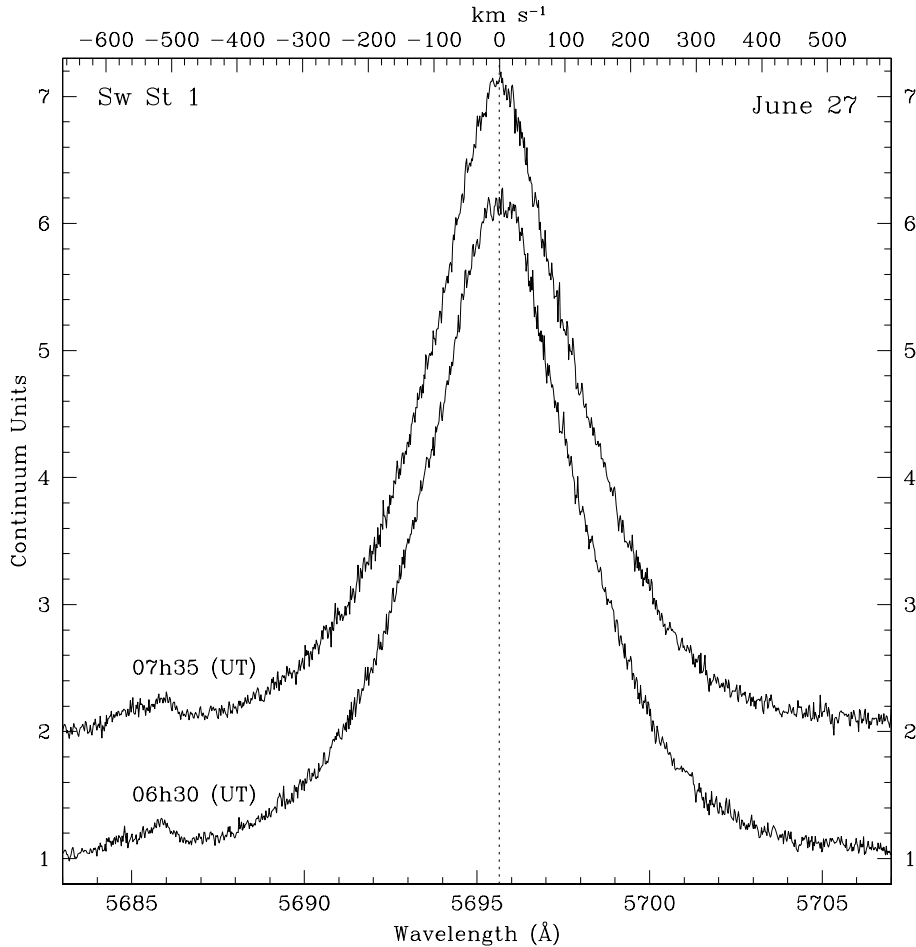


Fig. 12. Two consecutive spectra showing the C III λ 5696 emission line in Sw St 1 for 1997 June, 27. Velocities are given in the stellar rest frame.

(see Sect. 3.2.1). With an apparent $FWHM \approx 17 \text{ \AA}$, we infer $v_\infty \approx 800 \text{ km s}^{-1}$. Because the stellar continuum is underexposed, our $FWHM$ value is likely underestimated. Therefore, we expect $v_\infty \geq 800 \text{ km s}^{-1}$.

4.3. The [WC 9–10] nucleus of Sw St 1

This planetary nebula was discovered by Swings & Struve (1943). The central star of Sw St 1 is relatively bright and has been classified in the literature as [WC 9] or [WC 10]. Taking the usual C II:C III:C IV line strength ratio, Sw St 1 has been classified as [WC 9] by Leuenhagen & Hamann (1998) although the line strengths are unusually small compared to those of He 2-99 and BD +30°3639. Sw St 1 was included in the Méndez et al. (1991) work. In the latter study they did not find any spectral difference with massive WC 9 stars. With a terminal velocity of only $\approx 400 \text{ km s}^{-1}$ the central star of Sw St 1 appears to be a very peculiar [WC 9] star (Leuenhagen & Hamann 1998).

Fig. 12 show two consecutive spectra of the C III λ 5696 emission line in Sw St 1 for 1997 June 27. Surprisingly, this central star does not show any clear variability on top of the C III line. This could be attributed to either a true absence of wind variability, or to variations occurring on a time-scale shorter than the exposure time (60 min), or, more likely, longer than the 1-hour interval between the two exposures. This star needs to be

studied intensively in the future via spectroscopic monitoring. From the $FWHM$ of the C III λ 5696 emission line ($\sim 5.8 \text{ \AA}$), we estimate the terminal velocity to be only $\sim 300 \text{ km s}^{-1}$.

5. Discussion

The discrete stochastic component (made up of so-called “blobs” or “clumps”) observed for Population I WR stars seems to be well described by scaling laws relevant to supersonic, compressible turbulence in the wind (Henriksen 1994; Robert 1994). However, Lépine et al. (1996) showed that superposition effects of subpeaks compromise the detection of any possible scaling law, e.g. between flux and velocity dispersion of individual features observed on top of emission lines, as expected for a turbulent origin of the clumps. Nevertheless, the picture interpreting moving subpeaks as a set of density enhancements accelerated in WR winds (Robert 1992; Moffat et al. 1994) appears to be valid, now even for Population II [WC] stars.

The importance of ubiquitous wind clumping arising from WR PN nuclei cannot be overstated, as it imposes substantial constraints on the effective mass-loss rate (Moffat & Robert 1994) and might be the clue to understanding their origin and evolutionary status after passing the Asymptotic Giant Branch (AGB) stage: either a transition phase between AGB and PN stages (Le Bertre et al. 1989), or a post-AGB object suffering

a final thermal pulse (Rao 1987). Strong clumping, if it exists, would require at least revision of how the emitted flux, which depends on the square of the density (for recombination lines), is converted into mass, leading to significantly lower mass-loss rates by a factor of 3 or more (Moffat & Robert 1994; Hamann & Koesterke 1998; Hillier & Miller 1999). On the other hand, wind clumps may ultimately provide the necessary means of compression over several orders of magnitude and shielding required to form dust in some WR and nova winds (e.g. Marchenko, Moffat & Grosdidier 1999, and references therein) despite the high temperature of the expanding atmosphere.

In addition, wind clumping may affect the structure and dynamics of the surrounding circumstellar nebula and, therefore, provide a way to gain insight into the structure/nature of the different stages of mass-loss that the central star experiences during its own evolution. When taking into account the evolution of the velocity and mass loss rate of the present, fast WR wind, the interacting stellar wind model (Kwok et al. 1978) leads to considerably more structure on smaller scales compared to simulations where the fast wind is held stationary when encountering the previous slower, and denser AGB wind ejected about 10^3 years ago (Dwarkadas & Balick 1998 and references therein; Grosdidier et al. 1998). Moreover, the surrounding PN exhibits finite turbulent velocities in the particular case of [WC] nuclei. Spectroscopic modelling of the nebular lines with the Toruń code (see Gesicki et al. 1996; Acker et al. 2000b; Neiner et al. 2000) have shown that strong turbulent motions exist in nebulae with a [WC]-type nucleus. They suggest that the highly broadened profiles of the nebular lines may result from either strong variations of the expansion wind velocity, or clumping-enhanced instabilities at the interaction zone where the present fast, hot wind, catches up and collides with the slow, dense wind ejected by the star in its previous incarnation as an asymptotic red giant.

Furthermore, clumping questions the validity of the Standard Model of extended, WR atmospheres (see, e.g., Hillier 1995; Hamann 1995, and references therein), where stationary, spherically symmetric, *homogeneous* flows are assumed for simplicity along with an ad hoc, monotonic β -velocity law (see Castor & Lamers 1979). Preliminary attempts to take into account the effects of wind clumping on atmosphere models have been made by Hillier (1991), Schmutz (1997), Hamman & Koesterke (1998), and Hillier & Miller (1999).

6. Conclusion

In the first paper of this series, we have reported line-profile variations of optical, emission lines in four [WC 9–10]-type central stars of PN.

The major conclusions of this work are the following:

1. All the stars considered in this study show significant or marginal (object Sw St 1) line profile variations of their C III λ 5696 emission line, the best line to show this effect.
2. In the particular case of BD +30°3639, all the stellar emission lines within our spectral range are variable. The most

apparent subpeaks/gaps detected on the top of the C III line have *FWHM* ranging from ~ 1 – 4 \AA with a typical amplitude of about 4%–15% of the adjacent continuum flux. The amplitudes may have been as high as 20%–25% of the adjacent continuum flux during the strong outburst of 1997 July 26.

3. As was already noticed for massive WR stars, the blue-shifted absorption component of the lines exhibiting P-Cygni profiles in BD +30°3639 is significantly more variable than the emission component. This is likely mainly due to the small volume of matter in front of the stellar “disk”, a large fraction of which is subject to a higher level of coherent variability. This suggests linear sizes for the blobs of $\sim 1 R_*$.
4. The subpeaks normally show measurable velocity shifts in BD +30°3639 during their lifetime, but for some nights this is not the case. Subpeaks (or gaps) on the top of the C III line generally move from line center towards line edges in a symmetric fashion in the blue and red edges. This is consistent with wind features accelerated outward along radial trajectories.
5. The kinematics of 85 structures on top of the C III λ 5696 line of BD +30°3639 have been measured. Adopting $v_\infty = 700 \text{ km s}^{-1}$ and $R_* = 3.32 R_\odot$ the kinematics are well reproduced by a β -velocity law with $\beta \approx 3$, in contrast with the value $\beta = 1$ adopted in the atmosphere model. The line formation region is evaluated to span radial distances ~ 2 – $15 R_*$ from the central star. Within the accuracy of our acceleration measurements, $R_* = 3.32 R_\odot$ and $\beta = 3$ (hence $\beta R_* \approx 10$) seem to be good estimates of the stellar radius and of the β parameter: lower stellar radii would imply larger accelerations, which are not observed. However, lower stellar radii are more likely, requiring $\beta > 3$.
6. The lifetime of the subpeaks in BD +30°3639 is a few hours. This is consistent with the crossing time of mass through a zone limited to about a few tenths of the line formation region in radial extension. Thus the wind of BD +30°3639 is highly variable on a very short time-scale, which supports a turbulent origin.
7. The line variability of late-type [WC] nuclei is very similar to that observed in the massive WC 9 star WR 103 (see Robert 1992; Lépine & Moffat 1999). Thus, the wind fragmentation process appears to be a purely atmospheric wind phenomenon, despite the strong differences between both types of underlying hot stars.
8. We expect strong, hydrogen-deficient [WC] winds to be extreme examples for central stars of PN, so that any fine structure found in [WC] winds may apply to all winds of central stars of PN, much as one is finding now that weak, massive O-star winds also show the same fine structure as massive WR winds (Eversberg et al. 1998).

Acknowledgements. YG acknowledges financial aid from the French Ministry of Foreign Affairs. AFJM is grateful to NSERC (Canada) and FCAR (Québec) for financial support. AFJM acknowledges the award of a Killam Fellowship from the Canada Council for the Arts. We thank F. Cuisinier and S. Durand for their help in the data acquisition.

References

- Acker A., Marcout J., Ochsenbein F., Stenholm B., Tylenda R., 1992, The Strasbourg-ESO Catalogue of Galactic Planetary Nebulae. European Southern Observatory, Garching
- Acker A., Gorny S.K., Cuisinier F., 1996, *A&A* 305, 949
- Acker A., Grosdidier Y., Durand S., 1997, *A&A* 317, L51
- Acker A., Fresneau A., Pottasch S.R., Jasniewicz G., 1998, *A&A* 337, 253
- Acker A., Durand S., Parthasarathy M., Stenholm B., 2000a, *A&A* submitted
- Acker A., Gesicki K., Grosdidier Y., Szczerba R., Neiner C., 2000b, *A&A* in preparation
- Arnaud K., Borkowski K.J., Harrington J.P., 1996, *ApJ* 462, L75
- Balick B., Rodgers B., Hajian A., Terzian Y., Bianchi L., 1996, *AJ* 111, 834
- Blomme R., Runacres M.C., 1997, *A&A* 323, 886
- Brown J.C., Richardson L.L., Antokhin I., et al., 1995, *A&A* 295, 725
- Bryce M., Pedlar A., Muxlow T., Thomasson P., Mellema G., 1997, *MNRAS* 284, 815
- Castor J.I., Lamers H.G.J.L.M., 1979, *ApJS* 39, 481
- Dwarkadas V.V., Balick B., 1998, *ApJ* 497, 267
- Eversberg T., Lépine S., Moffat A.F.J., 1998, *ApJ* 494, 799
- Feibelman W.A., 1999, *ApJ* 519, 726
- Feldmeier A., 1995, *A&A* 299, 523
- Fullerton A.W., Gies D.R., Bolton C.T., 1996, *ApJS* 103, 475
- Gayley K.G., Owocki S.P., Cranmer S.R., 1995, *ApJ* 442, 296
- Gesicki K., Acker A., Szczerba R., 1996, *A&A* 309, 907
- Gillet D., Burnage R., Kholer D., et al., 1994, *A&AS* 108, 181
- Grosdidier Y., Acker A., Moffat A.F.J., Chesneau O., Dimeo T., 1997, In: Habing H.J., Lamers H.G.J.L.M. (eds.) *IAU Symp. 180, Planetary Nebulae*. Reidel, Dordrecht, p. 108
- Grosdidier Y., Moffat A.F.J., Joncas G., Acker A., 1998, *ApJ* 506, L127
- Grosdidier Y., Acker A., Moffat A.F.J., 2000, *A&A* submitted (Paper II)
- Hamann W.-R., 1995, In: van der Hucht K.A., Williams P.M. (eds.) *IAU Symp. 163, Wolf-Rayet Stars: Binaries, Colliding Winds, Evolution*. Kluwer, Dordrecht, p. 105
- Hamann W.-R., Koesterke L., 1998, *A&A* 335, 1003
- Harrington J.P., Lane N.J., White S.M., Borkowski K.J., 1997, *AJ* 113, 2147
- Henriksen R.N., 1994, *Ap&SS* 221, 25
- Hillier D.J., 1984, *ApJ* 280, 744
- Hillier D.J., 1991, *A&A* 247, 455
- Hillier D.J., 1995, In: van der Hucht K.A., Williams P.M. (eds.) *IAU Symp. 163, Wolf-Rayet Stars: Binaries, Colliding Winds, Evolution*. Kluwer, Dordrecht, p. 116
- Hillier D.J., Miller D.L., 1999, *ApJ* 519, 354
- Kaler J.B., Shaw R.A., Feibelman W.A., Lutz J.H., 1989, *ApJS* 70, 213
- Koesterke L., Hamann W.-R., 1997, *A&A* 320, 91
- Kwok S., Purton C.R., FitzGerald P.M., 1978, *ApJ* 219, L125
- Lamers H.G.J.L.M., Waters L.B.F.M., 1984, *A&A* 138, 25
- Le Bertre T., Heydari-Malayeri M., Epchtein N., Gouiffes C., Perrier C., 1989, *A&A* 225, 417
- Lépine S., Moffat A.F.J., 1999, *ApJ* 514, 909
- Lépine S., Moffat A.F.J., Henriksen R.N., 1996, *ApJ* 466, 392
- Leuenhagen U., Hamann W.-R., 1994, *A&A* 283, 567
- Leuenhagen U., Hamann W.-R., 1998, *A&A* 330, 265
- Leuenhagen U., Hamann W.-R., Jeffery C.S., 1996, *A&A* 312, 167
- Marchenko S.V., Moffat A.F.J., Grosdidier Y., 1999, *ApJ* 522, 433
- Méndez R.H., Herrero A., Manchado A., Kudritzki R.P., 1991, *A&A* 252, 265
- Moffat A.F.J., 1996, In: Vreux J.M., Detal A., Fraipont-Caro D., Gosset E., Rauw G. (eds.) *Wolf-Rayet Stars in the Framework of Stellar Evolution. Proc. 33rd Liège International Colloq., Univ. Liège, Inst. d'Astrophys., Liège*, p. 199
- Moffat A.F.J., 1995, In: van der Hucht K.A., Williams P.M. (eds.) *IAU Symp. 163, Wolf-Rayet Stars: Binaries, Colliding Winds, Evolution*. Kluwer, Dordrecht, p. 213
- Moffat A.F.J., Lépine S., Henriksen R.N., Robert C., 1994, *Ap&SS* 216, 55
- Moffat A.F.J., Robert C., 1994, *ApJ* 421, 310
- Neiner C., Acker A., Gesicki K., Szczerba R., 2000, *A&A* 358, 321
- Owocki S.P., 1994, *Ap&SS* 221, 3
- Owocki S.P., Castor J.I., Rybicki G.B., 1988, *ApJ* 335, 914
- Owocki S.P., Puls J., 1999, *ApJ* 510, 355
- Peña M., Stasińska G., Esteban C., et al., 1998, *A&A* 337, 866
- Rao N., Kameswara, 1987, *QJRAS* 28, 261
- Robert C., 1992, Ph.D. Thesis, Université de Montréal, Canada
- Robert C., 1994, *Ap&SS* 221, 137
- Robert C., Moffat A.F.J., Bastien P., Drissen L., St-Louis N., 1989, *ApJ* 347, 1034
- Runacres M.C., Blomme R., 1996, *A&A* 309, 544
- Sahai R., Trauger J.T., 1998, *ApJ* 116, 1357
- Schmutz W., 1997, *A&A* 321, 268
- Siebenmorgen R., Zijlstra A.A., Krügel E., 1994, *MNRAS* 271, 449
- Springmann U., 1994, *A&A* 289, 505
- Swings P., Struve O., 1943, *ApJ* 97, 194
- Torres A.V., Conti P.S., Massey P., 1986, *ApJ* 300, 379
- Tylenda R., Acker A., Stenholm B., 1993, *A&AS* 102, 595